



# EEG-Based Effective Connectivity Analysis for Attention Deficit Hyperactivity Disorder Detection Using Color-Coded Granger-Causality Images and Custom Convolutional Neural Network

Farhad Abedinzadeh Torghabeh<sup>1</sup> , Yeganeh Modaresnia<sup>1</sup> , Seyyed Abed Hosseini<sup>2\*</sup> 

<sup>1</sup>Department of Biomedical Engineering, Mashhad Branch, Islamic Azad University, Mashhad, Iran

<sup>2</sup>Department of Electrical Engineering, Mashhad Branch, Islamic Azad University, Mashhad, Iran

## Abstract

**Background:** Attention deficit hyperactivity disorder (ADHD) is prevalent worldwide, affecting approximately 8-12% of children. Early detection and effective treatment of ADHD are crucial for improving academic, social, and emotional outcomes. Despite numerous studies on ADHD detection, existing models still lack accuracy distinguishing between ADHD and healthy control (HC) children.

**Methods:** This study introduces an innovative methodology that utilizes granger causality (GC), a well-established brain connectivity analysis technique, to reduce the required EEG electrodes. We computed GC indexes (GCI) for the entire brain and specific brain regions, known as regional GCI, across different frequency bands. Subsequently, these GCIs were transformed into color-coded images and fed into a custom-developed 11-layer convolutional neural network.

**Results:** The proposed model is evaluated through a five-fold cross-validation, achieving the highest accuracy of 99.80% in the gamma frequency band for the entire brain and an accuracy of 98.50% in distinguishing the theta frequency band of the right hemisphere of ADHD and HC children by only using eight electrodes.

**Conclusion:** The proposed framework provides a powerful automated tool for accurately classifying ADHD and HC children. The study's outcome demonstrates that the innovative proposed methodology utilizing GCI and a custom-developed convolutional neural network can significantly improve ADHD detection accuracy, improving affected children's overall quality of life.

**Keywords:** Attention deficit hyperactivity disorder; Electroencephalography; Effective connectivity; Granger causality; Convolutional neural network.

**Received:** May 29, 2023 **Accepted:** October 10, 2023 **Published online:** November 13, 2023

**Citation:** Abedinzadeh Torghabeh F, Modaresnia Y, Hosseini SA. EEG-based effective connectivity analysis for attention deficit hyperactivity disorder detection using color-coded granger-causality images and custom convolutional neural network. Int Clin Neurosci J. 2023;10:e12. doi:10.34172/icnj.2023.12.

## Introduction

Approximately 8%-12% of children worldwide have attention deficit hyperactivity disorder (ADHD).<sup>1</sup> Three key characteristics of ADHD are inattention, hyperactivity, and impulsivity.<sup>2</sup> Autism spectrum disorder, learning disorders, bipolar disorder, externalizing problems, and sleep difficulties are often comorbid with ADHD. Furthermore, the disorder may contribute to mental health issues such as anxiety, depression, low self-esteem, suicide, substance abuse, and difficulties with sensory processing.<sup>2</sup> The early detection and treatment of ADHD are critical to effectively manage the condition and could improve academic, social, and emotional outcomes.<sup>3</sup>

The interaction and influence of various brain regions are referred to as brain connectivity. The difference between individuals with ADHD and others can be attributed to differences in brain function and connectivity.<sup>4</sup> Researchers have found that ADHD is associated with

altered levels of neurofunctional dependency across the cortex as well as altered connectivity across the whole brain and reduced structure-function coupling in feeder connections between hubs and peripheral regions.<sup>4,7</sup> It has been discovered that ADHD individuals exhibit weaker positive functional connectivity in fronto-striatal reward pathways, as well as stronger negative functional connectivity within prefrontal and visual reward pathways.<sup>4</sup> Various methods are available to study brain connectivity, such as structural and functional magnetic resonance imaging, *electroencephalography* (EEG), and multimodal imaging markers. Among them, EEG is an inexpensive, scalable, and portable technology that can be used to screen for disease even in areas without access to tertiary care facilities. In recent years, several studies have been conducted using EEG signals to investigate brain connectivity in ADHD, which suggests the effectiveness of this approach in providing a better understanding of



\*Correspondence to: Seyyed Abed Hosseini, Email: hosseini.s.ir@ieee.org

© 2023 The Author(s). This is an open access article distributed under the terms of the Creative Commons Attribution License (<http://creativecommons.org/licenses/by/4.0/>), which permits unrestricted use, distribution, and reproduction in any medium, provided the original work is properly cited.

ADHD and its effects on EEG analysis.

Kiiski and colleagues<sup>8</sup> investigated the relationship between functional EEG connectivity and ADHD symptoms. Using the weighted phase-lag index (WPLI) as a potential biomarker for ADHD diagnosis, they discovered that EEG connectivity in delta ( $\delta$ ), beta ( $\beta$ ), and gamma ( $\gamma$ ) bands effectively predicted hyperactive symptoms in the eyes-open resting state. Chen et al<sup>9</sup> examined ADHD and healthy control (HC) brain networks during the oddball P3 task by using EEG. They found that dysfunctional attention associated with ADHD occurred during the early stages of the task, as compared to HC. Furthermore, they suggested that this shortage could be caused by unusual information processing. Unlike ADHD, HCs exhibited significantly higher brain activity in the temporal and frontal regions during cortical activity analysis.

Ekhlesi et al<sup>10</sup> examined the unique information pathways of brain networks in ADHD compared to HC during an EEG-based attentional visual task. The effective connectivity between all scalp channels was determined using directed phase transfer entropy (dPTE) for all frequency bands. They revealed patterns of information transmission in the theta ( $\theta$ ) band, flowing from posterior to anterior regions in HC. Conversely, a disrupted pattern of information flow was observed in ADHD, characterized by an opposite flow direction. In another study, Ekhlesi et al<sup>11</sup> studied dPTE to measure effective connectivity between all scalp channels in ADHD and HC. Utilizing a multilayer artificial neural network (ANN) and genetic algorithm (GA) for feature selection, they could accurately differentiate between the  $\theta$  bands in the two groups with an accuracy of 89.7%.

Abbas and colleagues<sup>12</sup> used multichannel EEG recordings to examine effective connectivity within brain networks of ADHD and HC by using transfer entropy focusing on pair-wise directed information transfer between EEG electrodes across all frequency bands. Notably, the graph measures obtained from the estimated brain networks in the  $\beta$  band demonstrated the most significant differences between ADHD and HC.

Ekhlesi et al<sup>13</sup> investigated the impairments of brain connectivity in ADHD by using graph theory (GT) and directional information transfer. PTE was applied to calculate the weighted directed graphs, which were built from EEG signals of ADHD and HC. The local graph features from the  $\theta$  and  $\delta$  bands of HC and ADHD effectively differentiated the two groups using naïve Bayesian (NB), resulting in 91.2% and 90% accuracy, respectively. Moqadam et al<sup>14</sup> investigated the differences in connectivity patterns between ADHD and HC using EEG signals. The Katz fractal dimension of EEG was then used to extract the brain's connectivity networks (i.e., functionally connected regions) using the graph coloring algorithm. Their result revealed some disconnection

between the frontal and occipital lobes in ADHD, confirming that their anterior lobes are defective.

Coelli et al<sup>15</sup> compared the functional connectivity of ADHD and HC during Conners' "not-X" continuous performance test using the imaginary part of the coherence as a connectivity measure and GT analysis. Their findings supported the function of  $\theta$  and  $\beta$  rhythms in attention and concentration while indicating a less efficient network integration in ADHD. Talebi and Motie Nasrabadi<sup>16</sup> reported the EEG-based effective connectivity of ADHD compared to HC. They employed non-linear causal relationship estimation by ANN (nCREANN) and the direct Directed Transfer Function (dDTF) to examine the connection patterns. The dDTF analysis revealed that no unique frequency band could differentiate between the two groups, and various effective connection patterns were observed across all frequency bands. However, combining linear and non-linear connection measurements obtained from nCREANN enabled them to distinguish between the two groups with 99.07% accuracy.

Moghaddari et al<sup>17</sup> designed a 13-layer convolutional neural network (CNN) that utilized RGB color images derived from frequency sub-bands of EEG signals. Their approach achieved an accuracy of 98.48% in effectively distinguishing between ADHD and HC. Bakhtyari and Mirzaei<sup>18</sup> developed a convolutional long short-term memory (LSTM) model for ADHD detection. Their approach incorporated dynamic connectivity tensors from various frequency bands, where they achieved an accuracy of 99.7% in identifying ADHD.

The objective of this research is to investigate the distinct brain connectivity patterns exhibited by individuals with ADHD in comparison to those without the condition. This will be done by analyzing the causal interactions between brain regions using granger causality (GC).<sup>19</sup> A precise and efficient method will also be developed to detect ADHD accurately.

## Materials and Methods

The main framework of this study encompasses four key steps, as outlined below and depicted in [Figure 1](#).

- Pre-processing: The collected data undergoes pre-processing to enhance its quality and remove any unwanted artifacts or noise.
- Construction of directed GC Index (GCI) and directed regional GCI (rGCI): The aforementioned indexes are computed using the pre-processed data to investigate the causal relationships among the variables of interest.
- Construction of color-coded GCI and rGCI images.
- Construction of a novel CNN: A specialized CNN architecture was developed to classify GCI and rGCI images accurately. It underwent successful training and evaluation.

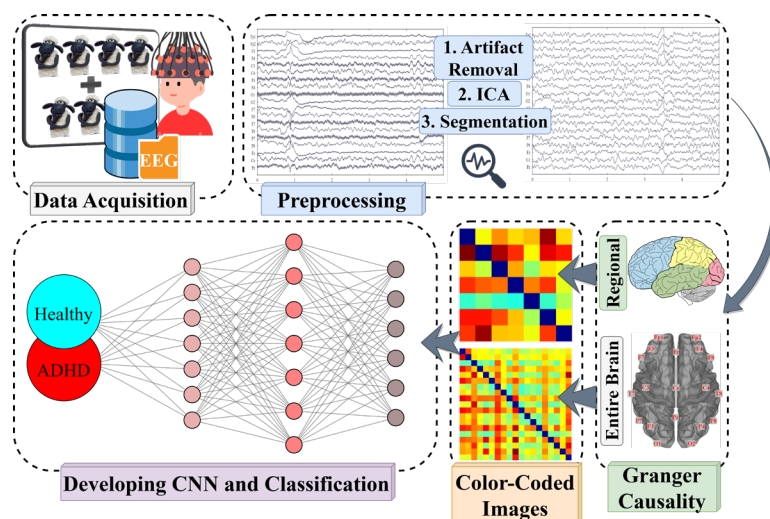


**Figure 1.** The Proposed Framework for ADHD Detection Using Regional and Universal GC With a Custom-Built CNN Architecture

### Database

In this research, we employed an openly accessible dataset from,<sup>20</sup> encompassing EEG recordings obtained from a cohort of 61 ADHD children and an additional 60 HC children, devoid of any documented psychological disorders. Throughout the visual attention task, EEG signals were recorded using 19 electrodes, adhering to the 10-20 standard international system, and sampled at a rate of 128 Hz. Two electrodes positioned in the earlobes were used to establish the reference points. The data recording process occurred within a soundproof environment, wherein the children were instructed to minimize any physical movements while the data was being captured. The children were presented with 20 images featuring visually appealing characters and were asked to count the number of characters in each image. Once the child responded to each image, the following image was displayed without delay. The duration of the EEG recording was determined by the child's performance, meaning that the recording continued until the completion of the task or the predetermined endpoint. Notably, the correctness or incorrectness of the child's answers was not considered during the recording process. A detailed description of the EEG signal and data acquisition protocol can be found in Motie Nasrabadi and colleagues' study.<sup>20</sup>

### Pre-processing

All pre-processing was performed using the EEGLAB toolbox<sup>21</sup> and MATLAB software. The initial step involved the application of a zero-phase band-pass finite impulse response (FIR) filter, ranging from 0.5 to 48 Hz, on the raw continuous EEG signals to effectively eradicate any interference caused by line noise. Next, the Clean Rawdata plugin<sup>22</sup> was employed to automatically eliminate any noticeable artifacts caused by electrode displacement in the data. The re-referencing procedure was followed,

utilizing a common average reference value across all channels. Subsequently, the EEG signals were subjected to independent component analysis to eliminate ocular, muscular, cardiac, and other artifacts. These components were then identified and excluded using the automatic ICLabel plugin.<sup>23</sup> After cleaning, the EEG signals were further filtered into conventional EEG bands of  $\delta$  (1–4 Hz),  $\theta$  (4–8 Hz), Alpha ( $\alpha$ ) (8–13 Hz),  $\beta$  (13–30 Hz), and  $\gamma$  (30–45 Hz), using five FIR filters based on the Kaiser window technique. Prior to segmenting the EEG data, this methodology was employed, which involved using a custom-made function. Subsequently, the time series was divided into epochs of 768 samples (equivalent to 6 seconds) for each subject. Since the recording durations differed across subjects, the total number of segments varied accordingly.

### Granger Causality

GC is a statistical concept that quantifies the predictive capacity of a particular time series on another.<sup>19</sup> It is a potent technique for identifying directed functional interactions from time-series data in neuroscience and neuroimaging, especially for characterizing functional circuits in the brain.<sup>24</sup> A viable approach for quantifying GCIs involves employing multivariate autoregressive (MVAR) models, wherein GCI can be computed based on the model's prediction errors. GCI effectively measures the causal relationship between variables by assessing the extent to which one variable's past values can predict another variable's values.<sup>25</sup> Mathematically, GCI is expressed as follows:

In this study, there is a 19-channel EEG data, let's denote it as  $X_1(t)$ ,  $X_2(t)$ , ...,  $X_{19}(t)$ , where  $t$  represents the time index. Our objective is to examine the causal relationship among these channels. To achieve this, we utilized an MVAR model that postulates each channel as a linear composition of its preceding values and the

preceding values of other channels. The MVAR model with order  $p$  can be mathematically represented as:

$$X_t = A_1 X_{t-1} + A_2 X_{t-2} + \dots + A_p X_{t-p} + \epsilon_t,$$

where  $X_t$  is a column vector containing the 19 channels at time  $t$ ,  $A_1, A_2, \dots, A_p$  are coefficient matrices to be estimated, and  $\epsilon_t$  represents the residual errors at time  $t$ . Subsequently, the parameters of the MVAR model need to be estimated using the provided EEG data. This process entails fitting the model for various orders ( $p$ ) and determining the optimal order that achieves a favorable trade-off between model complexity and data fit. The Akaike information criterion (AIC) is a prevalent criterion employed for model order selection, and it is defined as follows:

$$AIC(p) = -2 \ln(L(p)) + 2p,$$

where  $L(p)$  denotes the likelihood of the data given the model order  $p$ , while  $p$  signifies the number of parameters within the MVAR model. The AIC imposes penalties on models with greater complexity, thereby promoting the selection of more streamlined models that effectively capture the fundamental dynamics of the data. Upon identifying the optimal model order through AIC, the subsequent stage involves calculating GC between the channel pairs. This measurement quantifies the supplementary information contributed by the potential causal channel. GCI between channel  $X_i$  and channel  $X_j$  can be calculated using the following equation:

$$GC_{ij} = \log \frac{Var(\epsilon_i | H_0)}{Var(\epsilon_i | H_1)},$$

where  $Var(\epsilon_i | H_0)$  represents the variance of the residuals when both channels  $X_i$  and  $X_j$  are included in the model, and  $Var(\epsilon_i | H_1)$  represents the variance of the residuals when only channel  $X_i$  is included. The logarithm is applied to provide a symmetric measure of causality, and a positive value indicates a causal influence from  $X_j$  to  $X_i$ .

By evaluating GCI for every pair of channels, one can analyze the causal relationships inherent within the EEG data and determine which channels influence one another. This process allows for identifying and characterizing the directional interactions between the channels.<sup>26</sup> The GC value was computed for all possible pairwise combinations of channels, constructing a GC matrix for each segment within every frequency band, encompassing all subjects in the study. Additionally, in light of previous findings<sup>10,27</sup> indicating distinct anatomical and functional patterns of information flow within the brain hemispheres and regions, we have considered this by calculating rGCIs. To achieve this, the brain has been

divided into four regions: posterior, anterior, left, and right hemispheres. The division of these regions can be visualized in Figure 2, and further details are provided in Table 1. Subsequently, we transformed GCI and rGCI into color-coded images, where hotter colors represent stronger connectivity between pairs of nodes. This visual representation technique has been widely adopted to depict initial brain connectivity patterns.

### The Designed Convolutional Neural Network

Over the last decade, deep learning models have gained popularity due to their ability to accurately solve a wide range of problems. These models are a type of ANN that can analyze vast amounts of data and improve over time. A CNN can be designed to learn and extract meaningful patterns and relationships between the matrix elements in classifying GCI images. The rationales above prompted us to devise a deep neural network to categorize color-coded GCI images, eliminating the need for additional feature extraction in the GT analysis task. Our emphasis on creating a lightweight model allowed for efficient computation and resource management while maintaining sufficient complexity for accurate classification. We developed a lightweight CNN, comprising 11 layers and 165 100 learnable parameters. The proposed architecture (Figure 3) involved a combination of convolutional, pooling, normalization, and fully-connected (FC) layers. These layers enable the model to learn and effectively capture intricate dependencies within the data and facilitate extracting meaningful features and contributing to accurate classification outcomes.

**Table 1.** The Specific Channels Encompassed Within Each Brain Region for Calculating rGCI

Region	Channels
Anterior	Fp1, Fp2, F7, F3, Fz, F4, F8
Posterior	P7, P3, Pz, P4, P8, O1, O2
Right	Fp2, F4, F8, C4, T8, P8, P4, O2
Left	Fp1, F3, F7, C3, T7, P7, P3, O1

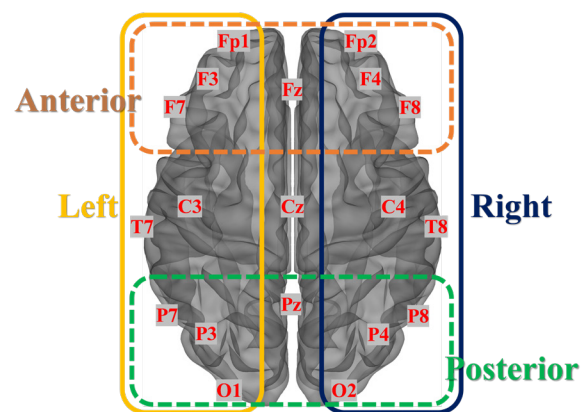


**Figure 2.** Division of Brain Regions for Calculating rGCI

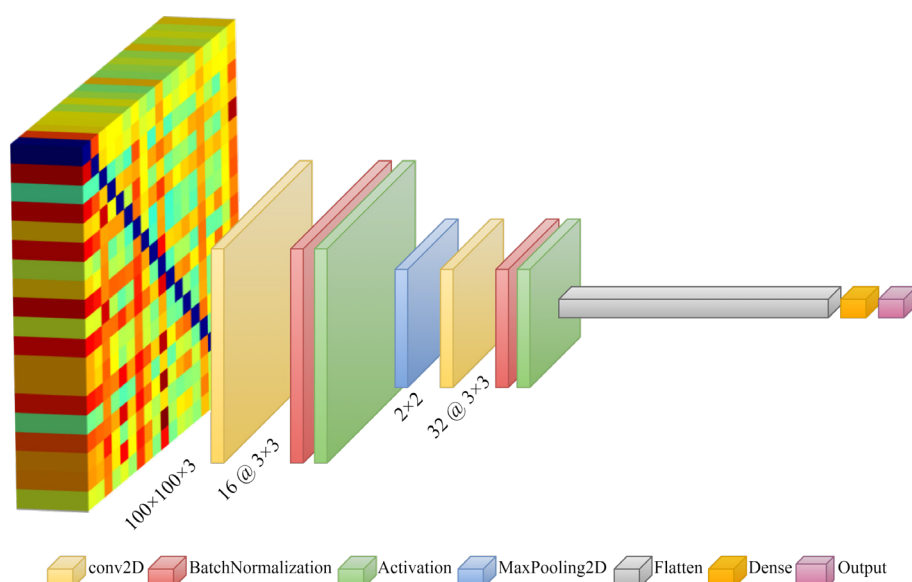


**Figure 3.** The Proposed 11-layer CNN Architecture, Including Convolutional, Normalization, Activation, Pooling, and FC Layers

Our proposed CNN comprises multiple layers, with the ImageInputLayer serving as the initial layer. This layer is designed to process  $100 \times 100$  RGB color-coded images. Following that, a convolutional layer is utilized, which plays a crucial role in identifying local patterns and capturing spatial relationships within connectivity matrices. Convolutional layers employ sliding convolutional filters to detect specific connectivity patterns, such as the strength or direction of connections between individual elements. This mechanism enables our custom-built CNN to analyze and interpret the matrix data effectively. Subsequently, a batch normalization layer, which aids in normalizing activations and diminishing internal covariate shifts, was utilized. The Rectified Linear Unit (ReLU) activation function is employed to introduce non-linearity and bolster the model's representational capabilities. Next, a max pooling layer with a  $2 \times 2$  pooling size and a stride of 2 is inserted to downsample the spatial dimensions and reduce the model's computational complexity. Pooling layers are employed to downsample the feature maps generated by the convolutional layers. This downsampling process helps reduce the spatial dimensions of the feature maps while retaining essential information. We used common pooling techniques of max pooling of  $2 \times 2$  size and a stride of 2, enabling CNN to select the maximum value within each pooling window.

Then, an additional convolutional layer characterized by a  $3 \times 3$  filter size and 32 filters are employed. Like the preceding convolutional layer, this layer is accompanied by a batch normalization layer and a ReLU activation function, which synergistically contribute to augmenting the model's performance. The output of this layer is flattened and then passed into an FC layer, which functions as a classifier. FC layers integrate the learned

features from the preceding layers and make predictions based on the relationships between these features. In classifying GCI images, the FC layers can effectively capture global patterns and make decisions based on the overall connectivity structure. The FC layers contribute to the network's ability to comprehend and classify complex connectivity patterns by leveraging the insights gained from the convolutional and pooling layers. In this case, we used an FC layer of 2 neurons to represent the ADHD and HC groups. To derive class probabilities, the SoftMax activation function is employed. A classification layer is then used to complete the classification task, which calculates the loss function and facilitates the overall classification by utilizing the predicted probabilities obtained from the previous layers. Table 2 summarizes the designed network architecture in detail.

The adaptive moment (Adam) estimation as a solver, an initial learning rate of 0.01, a maximum of 3 epochs, and 16 mini batches were set as the training options of this model. These parameters were selected during a trial-and-error procedure. We implemented a data shuffling technique at the beginning of each epoch to mitigate any potential bias in the training process. The default values for the remaining hyperparameters were used as specified by MATLAB.

Six evaluation metrics, including accuracy, sensitivity, specificity,  $F_1$  score, and area under curve (AUC), are calculated through a five-fold cross-validation (CV) technique to assess the model's performance and generalizability.

In this procedure, the GCI images associated with the segments and frequency band of ADHD and HC were divided into five subsets. During each iteration, one subset was designated for validation, while the remaining four subsets were utilized for training. This process was

repeated five times, with different subsets assigned for validation each time, and the evaluation metrics were calculated. Finally, the model’s performance on new and unseen data was evaluated comprehensively by averaging the results across the five iterations. This approach could also prevent overfitting and reasonably assess the model’s ability to generalize beyond the training data.

**Results**

In this study, EEG recordings obtained from a cohort of sixty-one ADHD children and an additional sixty HC children, both right-handed groups, with an average age of  $9.73 \pm 1.76$ , were analyzed. The AIC model order for ADHD and HC is summarized in Table 3 for different brain regions and frequency bands. The model order is selected as 4 in several frequency bands and regions, but in some areas and bands, the model order is determined to be 5 or 6. The group averages of GCI and rGCI, which were transformed into color-coded images, are illustrated in Figures 4 and 5, respectively. The hotter colors represent stronger connectivity between pairs of nodes, whereas the colder colors represent weak connectivity.

Table 4 provides a comprehensive summary of the classification results for each GCI and rGCI frequency band, presented as the mean and standard deviations

obtained from five-fold CV. In the classification of the entire brain, the  $\gamma$  band exhibited remarkably high accuracy, reaching 99.8%. This accuracy was accompanied by 100% sensitivity, 99.6% specificity, 99.6% precision, 0.99  $F_1$ , and an AUC of 1. Figure 6 shows confusion matrices for the performance of this frequency band and region, obtained through a five-fold CV technique. In the regional brain connectivity classification, the  $\theta$  band of the right hemisphere demonstrated the second-highest accuracy, achieving an impressive rate of 98.50%. Additionally, the results were further supported by a sensitivity of 99%, specificity of 98.80%, precision of 98.10%, an  $F_1$  score of 0.98, and an AUC of 0.99. The confusion matrices of this region and frequency obtained through a five-fold CV technique are illustrated in Figure 7.

**Table 2.** The Specifications Corresponding to the Developed CNN Layers

Layers	Specification
Image input	100 × 100 × 3
2D convolution	NumFilter = 16, Size = 3 × 3, Padding = Same
Batch normalization	Mean Decay = 0.1, Variance Decay = 0.1
ReLU	-
MaxPooling2D	Pool size = 2 × 2, Stride = 2 × 2
2D convolution	NumFilter = 32, Size = 3 × 3, Padding = Same
Batch normalization	Mean Decay = 0.1, Variance Decay = 0.1
ReLU	-
Flatten	-
Dense	2 Neurons (ADHD or HC)
Output	Loss function = Cross-entropy

**Table 3.** The AIC Model Order of ADHD and HC for Different Brain Regions and Frequency Bands

Region	Model Order									
	HC					ADHD				
	$\delta$	$\theta$	$\alpha$	$\beta$	$\gamma$	$\delta$	$\theta$	$\alpha$	$\beta$	$\gamma$
Entire brain	4	4	4	4	6	4	4	4	4	5
Posterior	4	4	4	5	4	4	4	4	4	5
Anterior	4	4	4	5	6	4	4	4	4	5
Right	4	4	4	4	6	4	4	4	4	6
Left	4	4	4	5	5	4	4	4	4	5

Note: The model order is utilized for calculating GCI.

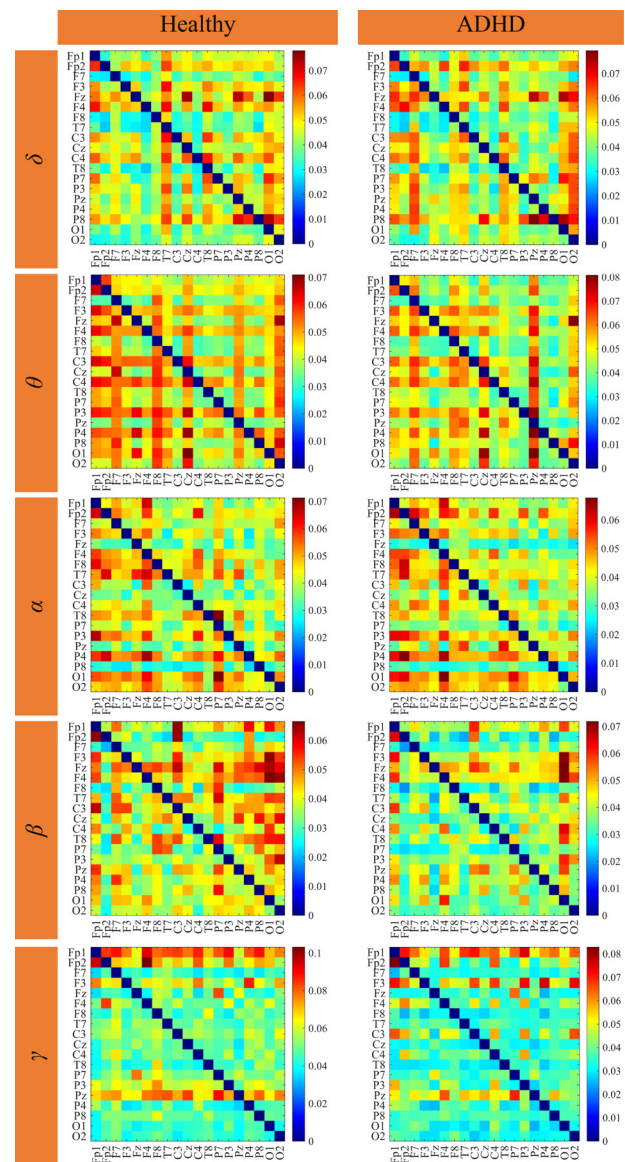
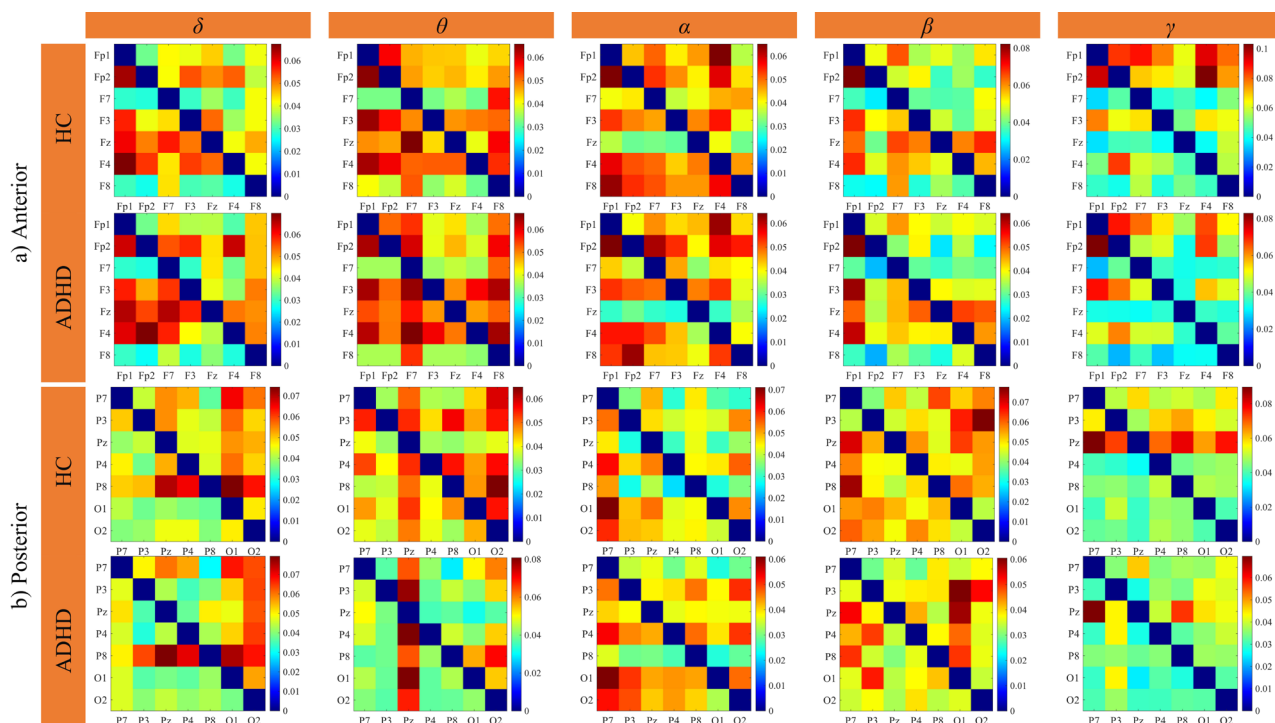


**Figure 4.** Color-Coded GCI Images Pertaining to Different Frequency Bands of ADHD and HC. The intensity of the color denotes a stronger connection between the nodes

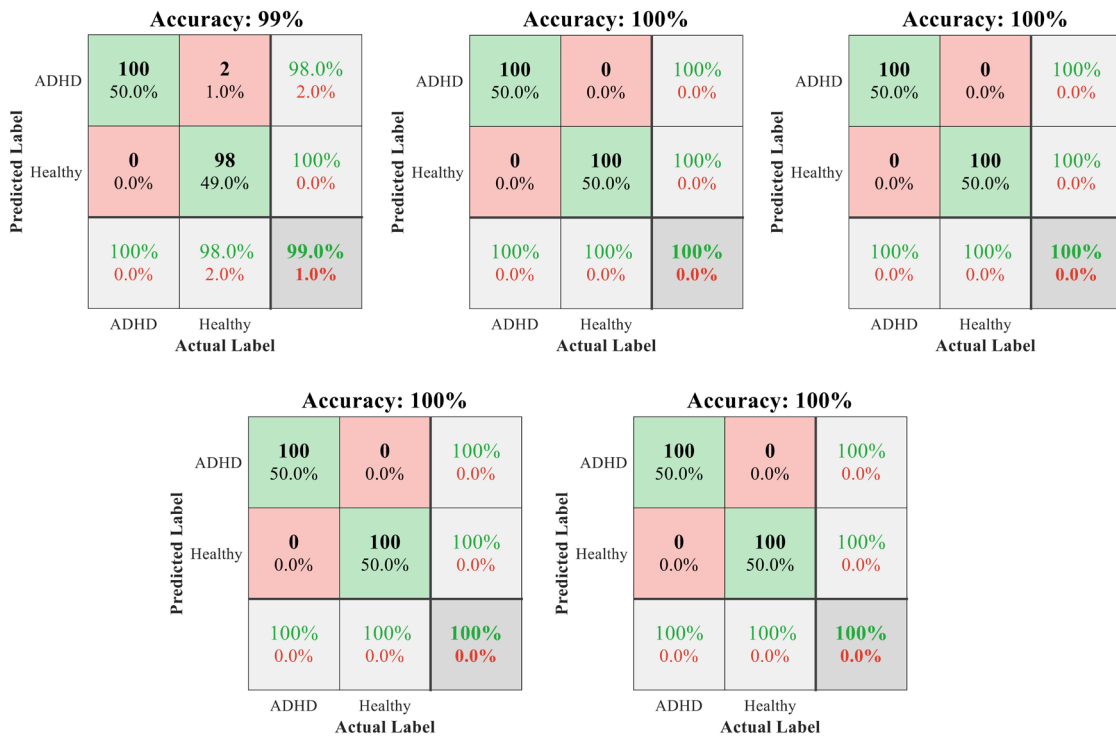
**Table 4.** The Classification Result of the ENTIRE BRAIN and Regional Parts in Each Frequency Band

Region	Band	Accuracy (%)	Sensitivity (%)	Specificity (%)	Precision (%)	F <sub>1</sub> score	AUC
Entire brain	$\delta$	99.10±1.02	99.80±0.44	98.40±2.19	98.46±2.10	0.99±0.01	0.99±0.00
	$\theta$	98.90±1.94	97.80±3.89	100	100	0.98±0.02	0.99±0.00
	$\alpha$	99.30±0.97	99.00±1.41	99.60±0.89	99.60±0.89	0.99±0.00	0.99±0.00
	$\beta$	99.10±0.65	99.40±1.34	99.80±1.30	98.82±1.26	0.99±0.00	0.99±0.00
	$\gamma$	<b>99.80±0.40</b>	<b>100</b>	<b>99.60±0.80</b>	<b>99.60±0.78</b>	<b>0.99±0.00</b>	<b>1</b>
Posterior	$\delta$	97.20±2.25	98.60±3.13	95.80±5.01	96.15±4.54	0.97±0.02	0.99±0.00
	$\theta$	92.10±6.57	95.80±4.91	88.40±15.82	90.79±11.14	0.92±0.05	0.98±0.01
	$\alpha$	96.40±1.29	96.40±5.12	96.40±3.57	96.61±3.33	0.96±0.01	0.99±0.00
	$\beta$	94.40±3.02	94.60±3.04	94.20±7.52	94.72±6.75	0.94±0.02	0.98±0.01
	$\gamma$	97.70±3.34	95.80±6.94	99.60±0.89	99.60±0.87	0.97±0.03	0.99±0.01
Anterior	$\delta$	94.00±8.48	97.20±2.68	90.80±18.41	93.29±12.89	0.94±0.06	0.99±0.00
	$\theta$	93.40±4.14	95.40±2.88	91.40±7.36	92.05±6.28	0.93±0.03	0.97±0.01
	$\alpha$	95.60±3.57	93.00±7.34	98.20±2.16	98.15±2.15	0.95±0.03	0.97±0.02
	$\beta$	98.20±1.39	97.40±2.50	99.00±0.70	98.98±0.72	0.98±0.01	0.99±0.00
	$\gamma$	96.90±1.98	95.80±4.60	98.00±1.58	98.00±1.55	0.96±0.02	0.99±0.01
Right	$\delta$	98.10±1.08	97.60±2.07	98.60±2.19	98.63±2.09	0.98±0.01	0.99±0.00
	$\theta$	<b>98.50±1.50</b>	<b>99.00±1.73</b>	<b>98.00±3.08</b>	<b>98.10±2.89</b>	<b>0.98±0.01</b>	<b>0.99±0.00</b>
	$\alpha$	98.50±1.87	100	97.00±3.74	97.18±3.43	0.98±0.01	0.99±0.01
	$\beta$	96.60±2.50	98.20±2.68	95.00±4.89	95.33±4.29	0.96±0.02	0.99±0.01
	$\gamma$	97.50±2.03	100	95.00±4.06	95.35±3.70	0.97±0.01	0.99±0.00
Left	$\delta$	96.30±2.25	98.40±3.57	94.20±5.54	94.72±4.93	0.96±0.02	0.99±0.01
	$\theta$	96.70±3.89	99.20±1.09	94.20±7.75	94.86±6.62	0.96±0.03	0.99±0.00
	$\alpha$	92.90±4.65	89.60±11.01	96.20±5.54	96.41±4.99	0.92±0.05	0.95±0.05
	$\beta$	96.60±3.02	98.80±2.16	94.40±6.42	94.94±5.66	0.96±0.02	0.99±0.00
	$\gamma$	95.40±5.97	99.60±0.89	91.20±12.07	92.69±9.08	0.95±0.05	0.99±0.00

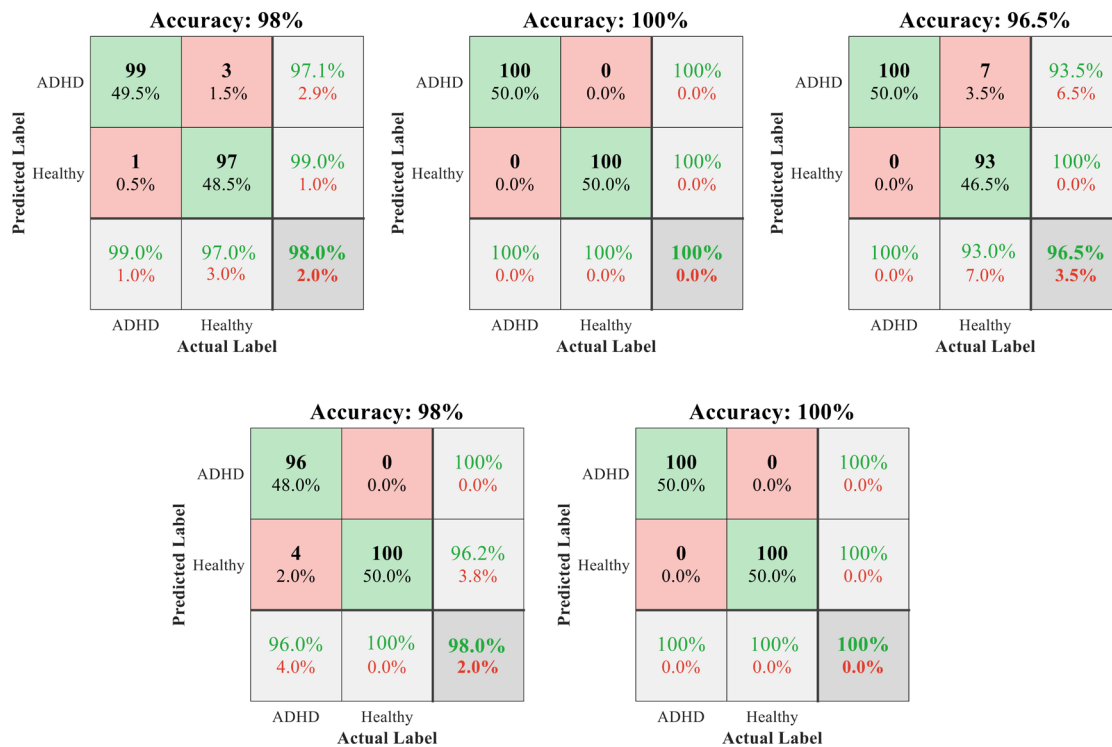
Note: The result is reported as mean±standard deviation of five-fold CV. The highest accuracy in the entire brain and regional part is highlighted in bold.



**Figure 5.** Color-Coded rGCI Images Pertaining to Different Frequency Bands of ADHD and HC in (a) Anterior, (b) Posterior, (c) Right, and (d) Left hemispheres



**Figure 6.** The confusion matrices of the  $\gamma$  band of the entire brain, during the five-fold CV technique, resulted in the best accuracy of 99.8 on average in the classification of the entire brain GCI



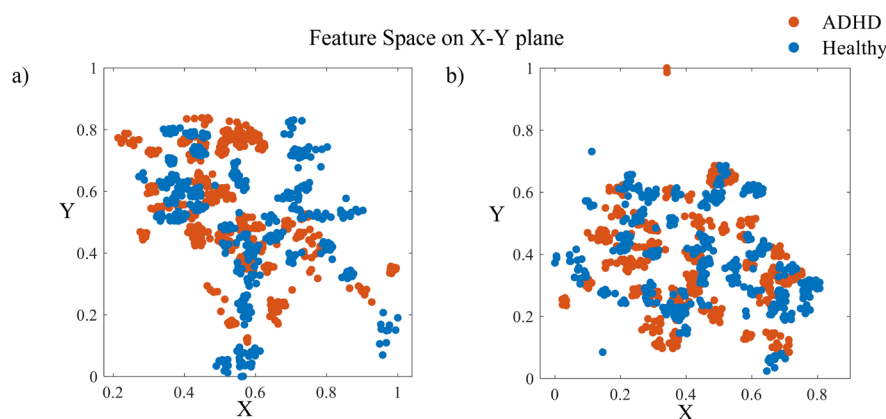
**Figure 7.** The confusion matrices of the  $\theta$  band of the right hemisphere, during the five-fold CV technique, resulted in the best accuracy of 98.5 on average in the classification of rGCI

Figure 8 illustrates the normalized extracted features obtained from color-coded GCI images of ADHD individuals and HC, achieving the highest classification accuracy in GCI and rGCI. These features are derived

from the latest convolutional layer before the FC layer.

**Discussion**

This study utilized color-coded images of brain connectivity to develop an innovative model distinguishing



**Figure 8.** The Extracted Features Obtained From the Color-Coded GCI Images on the X-Y Plane, Using the Best Models for Distinguishing Between Two Groups: (a)  $\gamma$  in the Entire Brain and (b)  $\theta$  in the Right Hemisphere

between HC and ADHD. These color-coded images were created using GC measures, representing the effective connectivity of brain regions. In light of previous studies highlighting distinct connectivity patterns between brain regions in the two groups, our study conducted GCI analyses on the entire brain and specific regional parts. Subsequently, the GCI matrices were transformed into color-coded images, which were prepared as input for the custom-designed 11-layer CNN. This transformation facilitated the integration of visual information into the CNN framework for further analysis and classification.

The proposed CNN architecture is meticulously designed to suit the classification of GCI color-coded images. Its layers are deliberately chosen to extract discernible features that hold significant utility in identifying Attention ADHD. The outcomes exhibit great promise, thereby furnishing a potent instrument for the automated categorization of ADHD and HC subjects. A collection of features that yielded optimal accuracy outcomes are visualized in Figure 8 to comprehend the mechanism and efficacy of feature extraction facilitated by this CNN. These features were particularly prominent within the  $\gamma$  band encompassing the entirety of the brain and within the  $\theta$  band localized to the right hemisphere. As illustrated in this figure, the proposed CNN effectively extracts features from color-coded images, resulting in distinct and well-separated clusters. This demonstrates CNN's significant potential for classifying ADHD and HC, consistently achieving more than 92% accuracy in all the regional parts, the entire brain, and their respective sub-bands.

The average accuracy rates across all frequency bands of various brain regions were impressive: 95.56% for the posterior region, 95.62% for the anterior region, 97.84% for the right hemisphere, and 95.58% for the left hemisphere. These results underscore the robustness and efficacy of the proposed framework, with the right hemisphere emerging as particularly adept at distinguishing between ADHD and HC.

**Table 5.** The Summary of the Current Studies Within the Field With the Same ADHD Dataset

Ref	Year	Method	Accuracy (%)
17	2020	13-layer CNN and color images of EEG	98.48
11	2021	dPTE, GA, and ANN	89.2
16	2022	nCREANN and dDTF	99.09
13	2022	PTE, GT, and NB classifier	91.2
18	2022	Convolutional LSTM	99.7
Proposed Method Color-coded GCI and rGCI images, and CNN			99.8

Table 5 comprehensively summarizes recent studies conducted on the same dataset. Our proposed framework outperformed these models despite their significant effort in methodology development. Notably, these studies exclusively examined and concentrated on the entire brain. In contrast, our investigation encompassed four distinct regional parts of the brain. The rationale behind this approach was to mitigate patient discomfort by minimizing the employed number of electrodes. To achieve this, the electrode count was substantially decreased from 19 to 7 electrodes in the anterior and posterior sections, and to 8 electrodes within the right and left hemispheres.

By incorporating regional components, two advantages are achieved: a decrease in computational expenses and the mitigation of discomfort stemming from employing large EEG electrodes. This, in turn, improves the overall viability of the real-time assessment method. Moreover, the findings indicate that even with the utilization of high-density EEG, relying on a limited quantity of electrodes for detecting ADHD remains reliable and economical. This reduction in electrode count, while upholding accuracy, presents a promising avenue in terms of practicality, cost-effectiveness, and implementation convenience.

## Conclusion

This study examined differences in how the brain

works and connects in people with ADHD, focusing on specific frequency bands. The study's results were quite impressive, with a 99.8% accuracy in the  $\gamma$  band across the entire brain. Notably, the right hemisphere, particularly in the  $\theta$  band, showed significant differences between ADHD and HC, resulting in 98.5% accuracy.

These findings suggest that the right hemisphere plays a crucial role in ADHD symptoms.

Future research directions could involve scaling this methodology to larger datasets and incorporating diverse cognitive tasks, potentially uncovering deeper insights into brain interactions. The success of this approach, combining streamlined architecture with color-coded connectivity images, holds promise for real-world applications and cost-effective diagnostic tools.

#### Acknowledgments

We extend our sincere appreciation to A. Motie Nasrabadi and his esteemed colleagues for generously providing their publicly accessible database. Their contribution has been invaluable to the progress and success of our research.

#### Authors' Contribution

Farhad Abedinzadeh Torghabeh conceived and developed the presented idea under the supervision of Seyyed Abed Hosseini. Farhad Abedinzadeh Torghabeh also carried out the material preparation and computations. He and Yeganeh Modaresnia drafted the initial version of the manuscript, which was subsequently reviewed and commented on by all authors. All authors contributed significantly to shaping the research, analysis, and manuscript, providing constructive feedback. Furthermore, all authors actively participated in every aspect of the investigation, including result analysis, visualization, and manuscript review. Finally, all authors have read and approved the final manuscript.

#### Code Availability

Code is available upon request from the corresponding author.

#### Competing Interests

The authors declare no conflict of interest.

#### Data Availability Statement

The utilized dataset can be accessed from the IEEE DataPort repository at the following address: <https://dx.doi.org/10.21227/rzfh-zn36>.

#### Ethical Approval

All procedures conducted in this research received approval from both the Institutional Review Board (IRB) and the Ethical Committee of Tehran University of Medical Sciences (TUMS). The participation of all subjects in the experiment was voluntary and informed written consent was obtained from the parents or legal guardians of each participant. Furthermore, the dataset utilized in this study, named the "EEG DATA FOR ADHD/CONTROL CHILDREN dataset," is publicly accessible through the following link: <https://ieee-dataport.org/open-access/eeg-data-adhd-control-children>, with the doi: 10.21227/rzfh-zn36.

#### Funding

No funds, grants, or other support were received for conducting

this study.

#### References

- Luo Y, Weibman D, Halperin JM, Li X. A review of heterogeneity in attention deficit/hyperactivity disorder (ADHD). *Front Hum Neurosci*. 2019;13:42. doi: [10.3389/fnhum.2019.00042](https://doi.org/10.3389/fnhum.2019.00042).
- Vashishtha S. Attention deficit hyperactivity disorder (ADHD): introduction, mental health concerns, and treatment. In: *New Developments in Diagnosing, Assessing, and Treating ADHD*. IGI Global; 2021. p. 23-41. doi: [10.4018/978-1-7998-5495-1.ch002](https://doi.org/10.4018/978-1-7998-5495-1.ch002).
- Feil EG, Small JW, Seeley JR, Walker HM, Golly A, Frey A, et al. Early intervention for preschoolers at risk for attention-deficit/hyperactivity disorder: preschool first step to success. *Behav Disord*. 2016;41(2):95-106. doi: [10.17988/0198-7429-41.2.95](https://doi.org/10.17988/0198-7429-41.2.95).
- Rohr CS, Bray SL, Dewey DM. Functional connectivity based brain signatures of behavioral regulation in children with ADHD, DCD, and ADHD-DCD. *Dev Psychopathol*. 2023;35(1):85-94. doi: [10.1017/s0954579421001449](https://doi.org/10.1017/s0954579421001449).
- Hamed N, Khadem A, Delrobaei M, Babajani-Feremi A. Detecting ADHD based on brain functional connectivity using resting-state MEG signals. *Front Biomed Technol*. 2022;9(2):110-8. doi: [10.18502/fbt.v9i2.8850](https://doi.org/10.18502/fbt.v9i2.8850).
- Aydın S, Çetin FH, Uytun MÇ, Babadağı Z, Güven AS, Işık Y. Comparison of domain specific connectivity metrics for estimation brain network indices in boys with ADHD-C. *Biomed Signal Process Control*. 2022;76:103626. doi: [10.1016/j.bspc.2022.103626](https://doi.org/10.1016/j.bspc.2022.103626).
- Hearne LJ, Lin HY, Sanz-Leon P, Tseng WI, Gau SS, Roberts JA, et al. ADHD symptoms map onto noise-driven structure-function decoupling between hub and peripheral brain regions. *Mol Psychiatry*. 2021;26(8):4036-45. doi: [10.1038/s41380-019-0554-6](https://doi.org/10.1038/s41380-019-0554-6).
- Kiiski H, Rueda-Delgado LM, Bennett M, Knight R, Rai L, Roddy D, et al. Functional EEG connectivity is a neuromarker for adult attention deficit hyperactivity disorder symptoms. *Clin Neurophysiol*. 2020;131(1):330-42. doi: [10.1016/j.clinph.2019.08.010](https://doi.org/10.1016/j.clinph.2019.08.010).
- Chen C, Yang H, Du Y, Zhai G, Xiong H, Yao D, et al. Altered functional connectivity in children with ADHD revealed by scalp EEG: an ERP study. *Neural Plast*. 2021;2021:6615384. doi: [10.1155/2021/6615384](https://doi.org/10.1155/2021/6615384).
- Ekhlas A, Motie Nasrabadi A, Mohammadi MR. Direction of information flow between brain regions in ADHD and healthy children based on EEG by using directed phase transfer entropy. *Cogn Neurodyn*. 2021;15(6):975-86. doi: [10.1007/s11571-021-09680-3](https://doi.org/10.1007/s11571-021-09680-3).
- Ekhlas A, Motie Nasrabadi A, Mohammadi M. Classification of the children with ADHD and healthy children based on the directed phase transfer entropy of EEG signals. *Front Biomed Technol*. 2021;8(2):115-22. doi: [10.18502/fbt.v8i2.6515](https://doi.org/10.18502/fbt.v8i2.6515).
- Abbas AK, Azemi G, Amiri S, Ravanshadi S, Omidvarnia A. Effective connectivity in brain networks estimated using EEG signals is altered in children with ADHD. *Comput Biol Med*. 2021;134:104515. doi: [10.1016/j.compbimed.2021.104515](https://doi.org/10.1016/j.compbimed.2021.104515).
- Ekhlas A, Motie Nasrabadi A, Mohammadi M. Analysis of EEG brain connectivity of children with ADHD using graph theory and directional information transfer. *Biomed Tech (Berl)*. 2023;68(2):133-46. doi: [10.1515/bmt-2022-0100](https://doi.org/10.1515/bmt-2022-0100).
- Moqadam R, Loghmani N, Khorrami Moghaddam A, Allahverdy A. Differentiating brain connectivity networks in ADHD and normal children using EEG. In: 2022

- 30th International Conference on Electrical Engineering (ICEE). Tehran, Iran: IEEE; 2022. p. 231-5. doi: [10.1109/icee55646.2022.9827093](https://doi.org/10.1109/icee55646.2022.9827093).
15. Coelli S, Calcagno A, Iacone E, Gaspari L, Canevini MP, Bianchi AM. Sustained attention task-related changes of functional connectivity in children with ADHD. In: 2022 IEEE 21st Mediterranean Electrotechnical Conference (MELECON). Palermo, Italy: IEEE; 2022. p. 585-9. doi: [10.1109/melecon53508.2022.9842899](https://doi.org/10.1109/melecon53508.2022.9842899).
  16. Talebi N, Motie Nasrabadi A. Investigating the discrimination of linear and nonlinear effective connectivity patterns of EEG signals in children with attention-deficit/hyperactivity disorder and typically developing children. *Comput Biol Med.* 2022;148:105791. doi: [10.1016/j.compbimed.2022.105791](https://doi.org/10.1016/j.compbimed.2022.105791).
  17. Moghaddari M, Zolfy Lighvan M, Danishvar S. Diagnose ADHD disorder in children using convolutional neural network based on continuous mental task EEG. *Comput Methods Programs Biomed.* 2020;197:105738. doi: [10.1016/j.cmpb.2020.105738](https://doi.org/10.1016/j.cmpb.2020.105738).
  18. Bakhtyari M, Mirzaei S. ADHD detection using dynamic connectivity patterns of EEG data and ConvLSTM with attention framework. *Biomed Signal Process Control.* 2022;76:103708. doi: [10.1016/j.bspc.2022.103708](https://doi.org/10.1016/j.bspc.2022.103708).
  19. Granger CWJ. Investigating causal relations by econometric models and cross-spectral methods. *Econometrica.* 1969;37(3):424-38. doi: [10.2307/1912791](https://doi.org/10.2307/1912791).
  20. Motie Nasrabadi A, Allahverdy A, Samavati M, Mohammadi M. EEG Data for ADHD/Control Children. IEEE DataPort; 2020. Available from: <https://ieee-dataport.org/open-access/eeg-data-adhd-control-children>.
  21. Delorme A, Makeig S. EEGLAB: an open source toolbox for analysis of single-trial EEG dynamics including independent component analysis. *J Neurosci Methods.* 2004;134(1):9-21. doi: [10.1016/j.jneumeth.2003.10.009](https://doi.org/10.1016/j.jneumeth.2003.10.009).
  22. Delorme A. Clean Raw Data Plugin. Available from: [https://github.com/scn/clean\\_rawdata](https://github.com/scn/clean_rawdata).
  23. Pion-Tonachini L, Kreutz-Delgado K, Makeig S. ICLABEL: an automated electroencephalographic independent component classifier, dataset, and website. *Neuroimage.* 2019;198:181-97. doi: [10.1016/j.neuroimage.2019.05.026](https://doi.org/10.1016/j.neuroimage.2019.05.026).
  24. Seth AK, Barrett AB, Barnett L. Granger causality analysis in neuroscience and neuroimaging. *J Neurosci.* 2015;35(8):3293-7. doi: [10.1523/jneurosci.4399-14.2015](https://doi.org/10.1523/jneurosci.4399-14.2015).
  25. Schmidt C, Pester B, Schmid-Hertel N, Witte H, Wismüller A, Leistriz L. A multivariate granger causality concept towards full brain functional connectivity. *PLoS One.* 2016;11(4):e0153105. doi: [10.1371/journal.pone.0153105](https://doi.org/10.1371/journal.pone.0153105).
  26. Wismüller A, Dsouza AM, Vosoughi MA, Abidin A. Large-scale nonlinear Granger causality for inferring directed dependence from short multivariate time-series data. *Sci Rep.* 2021;11(1):7817. doi: [10.1038/s41598-021-87316-6](https://doi.org/10.1038/s41598-021-87316-6).
  27. Wang S, Zhang D, Fang B, Liu X, Yan G, Sui G, et al. A study on resting EEG effective connectivity difference before and after neurofeedback for children with ADHD. *Neuroscience.* 2021;457:103-13. doi: [10.1016/j.neuroscience.2020.12.038](https://doi.org/10.1016/j.neuroscience.2020.12.038).